Dynamics and Kinetics of the S + HO_2 Reaction: A Theoretical Study

M. Y. BALLESTER, A. J. C. VARANDAS

Departamento de Química, Universidade de Coimbra, 3004-535 Coimbra, Portugal

Received 10 November 2007; revised 22 January 2008; accepted 22 January 2008

DOI 10.1002/kin.20340
Published online in Wiley InterScience (www.interscience.wiley.com).

ABSTRACT: We report a quasi-classical trajectory study of the S + HO_2 reaction using a previously reported global potential energy surface for the ground electronic state of HSO_2. Zero-point energy leakage is approximately accounted for by using the vibrational energy quantum mechanical threshold method. Calculations are carried out both for specific ro-vibrational states of the reactants and thermalized ones, with rate constants being reported as a function of temperature. The results suggest that the title reaction is capture type, with OH and SO showing as the most favorable products. The internal energy distribution of such products and the reaction mechanism are also investigated. © 2008 Wiley Periodicals, Inc. Int J Chem Kinet 40: 533–540, 2008

INTRODUCTION

Sulfur is an important element when studying atmospheric chemistry [1]. In turn, the mercapto radical (HS) has been observed in interstellar space [2], whereas sulfur compounds are also known to play an important role in combustion chemistry [3]. However, owing to the large number of electrons involved, high-level theoretical studies involving sulfur atoms are somewhat limited due to being computationally too expensive. In previous works of this series [4,5], we have reported full dynamics studies involving the title sulfur-containing species by using a global double many-body expansion (DMBE [6,7]) potential energy surface reported elsewhere [8]. All these studies have employed the quasi-classical trajectory (QCT) method, a technique that will be also adopted in the current study. In fact, the good agreement previously achieved when comparing our predictions with available experimental results suggests that both the HSO_2 DMBE potential energy surface and the dynamics approach should be reliable for our purposes in this work.

Although the title reaction should play a role whenever sulfur atoms (the ground electronic state of atomic sulfur is implied heretofore) are present in the atmosphere, no dynamics study of it has yet been reported in the open literature. Our aim in the present work is to extend the series of previous studies to the reaction

$$S + HO_2 \rightarrow \text{products} \qquad (1)$$

by using QCT and the above-mentioned DMBE potential energy surface. Thus, we will ignore both quantum effects (except for those related with the reactant triatomic molecule whose initial state is mimicked as closely as possible) and nonadiabaticity. Given the large masses of the reactant species and the fact that the ground (^3P) and first-excited (^1D) electronic states are separated by more than 25 kcal mol^{-1} [9], we can

Correspondence to: A. J. C. Varandas; e-mail: varandas@qtvs1.qui.uc.pt.

Contract grant sponsor: Fundação para a Ciência e a Tecnologia, Portugal, under POCI 2010 of Quadro Comunitário de Apoio III co-financed by FEDER

hardly judge such effects to have any crucial role for the rate constant calculations carried out in the present work. The paper is organized as follows. The next section reviews the potential energy surface, whereas the utilized computational methods are described in the following section. The results will be presented and discussed in the penultimate section, and the major conclusions gathered in the last section.

POTENTIAL ENERGY SURFACE

All calculations here performed have employed our six-dimensional DMBE potential energy surface published elsewhere [8] for the electronic ground state of HSO_2. It employs previously reported forms of the same type for the diatomic and triatomic fragments ([8] and references therein), and four-body energy terms that were parameterized to mimic CASPT2/FVCAS/AVXZ ($X = D, T$) calculations for the tetratomic system. In this section, we illustrate its major features that are of interest for the title reaction.

Figure 1 displays the minimum energy path (MEP) for the formation of OH + SO from S + HO_2, whereas Fig. 2 represents the MEP for HOS formation. Other products are allowed for such reactants but the illustrated here are the most favorable ones. According to energetics of the surface (see Table 1 and Fig. 11 of

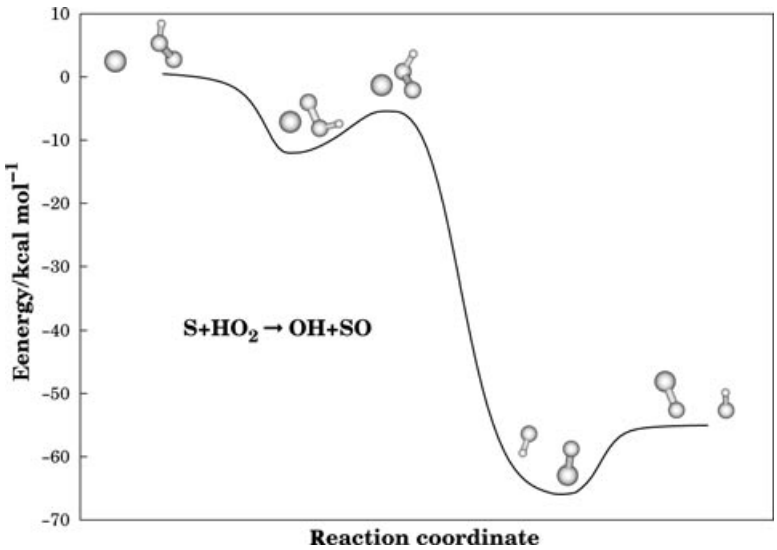

Figure 1 Minimum energy path for the reaction S + HO_2 → OH + SO according to the potential energy surface used in this work.

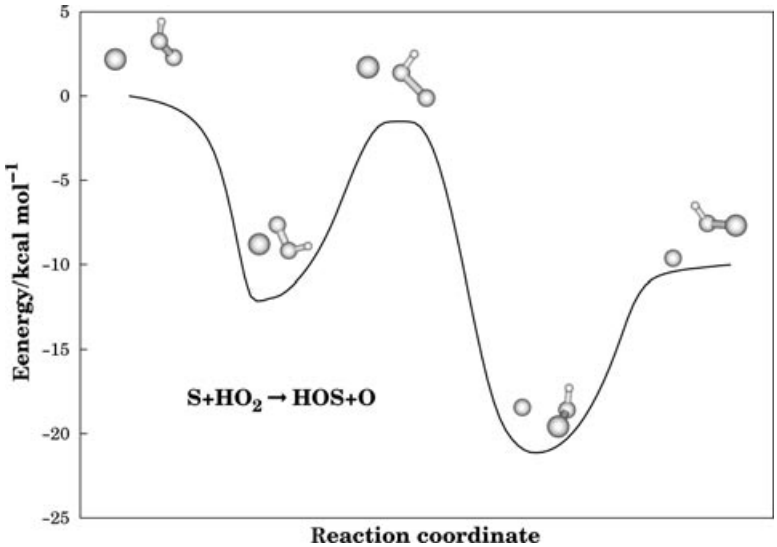

Figure 2 Minimum energy path for the reaction S + HO_2 → HOS + O according to the potential energy surface used in this work.

[8]), the H + SO_2 channel lies 84.4 kcal mol^{-1} below the reactants.*

Figures 1 and 2 also show a common four-body intermediate structure, HOO···S. The relatively large well depth of this adduct (12.2 kcal mol^{-1}) is directly linked to the two attractive SO interactions (5.1 and 7.1 kcal mol^{-1}), since the repulsive three-body contributions involving the sulfur atom, as well as four-body ones, are irrelevant for such an arrangement. Although such a species could in principle be isolated, coming from S + HO_2 yields an extra energy of 5.6 kcal mol^{-1} that must be removed from the moiety such as to allow stabilization and avoid decaying into other species. To our knowledge, no evidence has yet been reported about its existence.

COMPUTATIONAL PROCEDURES

To run the trajectories, we have utilized an adapted version of the VENUS [10] code, which accommodates the HSO_2 DMBE potential energy surface [8]. The step size used for the numerical integrations was 2.5×10^{-16} s, warranting a conservation of the total energy to better than 2 parts in 10^4. Two types of calculations have been carried out. First, we have run trajectories for fixed ro-vibrational combinations of the reactants (HO_2) such as to provide a detailed understanding of the reaction mechanism. Then, thermalized calculations have been performed to directly assert the rate constant.

The calculations for specific ro-vibrational states have been carried out for translational energies over the range $0.2 \leq E_{tr}/\text{kcal mol}^{-1} \leq 10.0$, with the hydroperoxyl radical kept in its ground vibrational state [11] ($v_1 = 0$, $v_2 = 0$, $v_3 = 0$), and the rotational energy for each principal axis fixed at $RT/2$ with $T = 300$ K. Following the usual practice, batches of 100 trajectories per collisional energy have been run to determine the maximum impact parameter (b_{max}) that leads to reaction. For a given translational energy, reactive cross sections were then calculated from $\sigma_r = \pi b_{max}^2 P_r$ and the associated 68% uncertainties from $\Delta\sigma_r = \sigma_r[(N_T - N_r)/(N_T N_r)]^{\frac{1}{2}}$, where N_r is the number of reactive trajectories in a total of N_T, $P_r = N_r/N_T$ is the reactive probability, and b_{max} is the maximum impact parameter.

From the reactive cross section assuming a Maxwell–Boltzmann distribution over the translational energy (E_{tr}), the specific thermal rate coefficient is obtained as

$$k(T) = g_e(T)\left(\frac{2}{k_B T}\right)^{3/2}\left(\frac{1}{\pi\mu}\right)^{1/2}\int_0^\infty E_{tr}\sigma(E_{tr}) \times \exp\left(-\frac{E_{tr}}{k_B T}\right) dE_{tr} \quad (2)$$

where T is the temperature, k_B is the Boltzmann constant, μ the reactants reduced mass, and

$$g_e(T) = 1/[5 + 3\exp(-570/T) + \exp(-825/T)] \quad (3)$$

accounts in the usual way [12,13] for the electronic degeneracies of the reactants [$S(^3P) + HO_2(^2A'')$] and the fact that the DMBE potential energy surface refers to a doublet. The atomic levels of sulfur have been taken from the NIST database [14].

We now address the problem of ZPE leakage, which is well known in QCT theory. Both "active" and "nonactive" methods have been suggested ([15] and references therein) to account for it in an approximate manner. In the nonactive methods such as the one [16] here utilized, trajectories leading to aphysical products (with vibrational/internal energies below a given threshold) are thrown out and eventually replaced [17] by running novel trajectories. The perturbed statistics may then be corrected a posteriori [18]. Thus, no trajectory calculations, besides those run in the traditional QCT method, are required. Specifically, in $VEQMT_C$ [16] we consider as physical only the outcomes where the total vibrational energy is larger than the sum of their ZPEs [16], an approach that has also been employed in previous work [4]. Clearly, $VEQMT_C$ [16] and other similar methods (including active ones [15] where a constraint is introduced to prevent the trajectories from entering the region of phase space that allows vibrational modes to have less than its ZPE) will not be free from ambiguity, an issue that will not be addressed any further in the present work. Suffice it to say that accounting for ZPE tends to enhance reactivity for the title reaction (see later).

The second series of calculations refers to thermalized ones. The collisional energy is then selected from a Maxwell–Boltzmann distribution by using the cumulative function:

$$G(E_{tr}) = \left(\frac{1}{k_B T}\right)^2 \int_0^{E_{tr}} E'_{tr}\exp(-E'_{tr}/k_B T)\, dE'_{tr} \quad (4)$$

where E_{tr} is chosen randomly for each trajectory by solving the equation $G(E_{tr}) - \xi = 0$, where ξ ($0 \leq \xi \leq 1$) is a random number. In turn, as in [5], the vibrational quantum numbers $v = v_1, v_2, v_3$ of the HO_2

*Energies in this paragraph do not include the zero-point energy (ZPE).

were sampled by using the cumulative distribution function

$$C(E_v) = \sum_{n=0}^{v} P(n) \tag{5}$$

where $P(n)$ has been chosen to be the Boltzmann distribution. With the dependence of the vibrational energy (E_v) on the quantum number of HO_2 being reported elsewhere [19], the specification of the initial internal energy is completed by specifying a standard thermal distribution for the rotational energy [10] (for this, we considered the reactants triatom as a symmetric top). After optimizing the maximum impact parameter as described above, the thermalized rate constant is calculated from

$$k(T) = g_e(T) \left(\frac{8k_B T}{\pi \mu} \right)^{1/2} \pi b_{\max}^2 \frac{N_r}{N_T} \tag{6}$$

where all symbols have the meaning assigned in preceding paragraphs. Similarly, the associated uncertainty has been calculated using an analogue of the expression used above for the cross section. For production, batches of 5000 trajectories were judged sufficient for the thermalized calculations (at $T = 300$, 1000, and 1500 K), whereas batches of 2000 trajectories were run at each translational energy for specific calculations.

The procedure used to assign the reaction products is the same as in previous studies [20]. Although there are 14 possible channels in an atom + triatom collisional process (the various isomers of a given species are assumed indistinguishable), we note that according to the energetics of the potential energy surface [8] there is no direct connection between the reactants and the HSO + O channel. This issue has been checked in detail by running two batches of 100 trajectories for specific calculations at translational energies of 0.2 and 10.0 kcal mol^{-1}. In both cases, formation of HSO has not been observed, with HOS being formed instead. Note that HOS refers to a structure with a central oxygen atom bonded to sulfur and hydrogen. This isomer differs therefore from HSO in that the central atom in the latter is sulfur: such a structure corresponds to the global minimum [21], with an energy difference of 0.9 kcal mol^{-1} separating those two species. Accordingly, we have modified the assignment of channels 5 and 6 used in our previous work [4] such as to identify the corresponding HOS + O ones.

RESULTS AND DISCUSSION

Table I collects the results of the specific calculations, both of pure QCT and $VEQMT_C$ types. All symbols have the meaning assigned above, with N_T indicating the total number of trajectories run in each method, and $N_r = \sum_x N_r^x$ the total number of reactive ones. Headings of other columns specify the number of reactive trajectories for the corresponding x products. As seen, the OH and SO products are by far the most formed ones, followed by HOS and O in a 5:1 ratio. For completeness, we also show SO_2 formation, even if it is an almost negligible process.

The results for thermalized calculations are similarly presented in Table II. There, the total number of trajectories for QCT is reported to recall that some of the 5000 trajectories run did not converge, i.e., have not led to any of the possible products after 4×10^5 iterations. This has also occurred in previous work [4], when some of the trajectories were captured into the deep well associated with the HOSO species and persisted there until a prespecified maximum number of iterations were reached.

When the $VEQMT_C$ criterion is utilized, a considerable number of nonreactive trajectories is disregarded,

Table I Results of Specific Trajectories Calculations for[a] S + HO_2

E_{tr}	b_{max}	QCT				$VEQMT_C$				
(kcal mol^{-1})	(Å)	$\sum_x N_r^x$	$x = H + SO_2$	OH + SO	O + HOS	N_T	$\sum_x N_r^x$	$x = H + SO_2$	OH + SO	O + HOS
0.2	8.7	492	15	405	72	639	483	15	405	63
0.5	7.3	405	5	326	74	577	393	5	325	63
1.0	6.4	342	7	274	61	595	335	7	273	55
1.5	6.0	299	5	236	58	637	296	5	236	55
2.0	5.2	339	7	259	73	733	333	7	259	67
3.0	4.9	304	3	238	63	784	301	3	238	60
5.0	4.3	307	6	235	66	964	299	6	235	58
10.0	3.5	360	7	274	79	1144	355	7	274	74

[a] The total number of trajectories in QCT is $N_T = 2000$ for all translational energies.

Table II Results of Thermalized Calculations for the Title Reaction

T	b_{max}	QCT					VEQMT$_C$				
(K)	(Å)	N_T	$\sum_x N_r^x$	$x = H + SO_2$	OH + SO	O + HOS	N_T	$\sum_x N_r^x$	$x = H + SO_2$	OH + SO	O + HOS
300	8.0	5000	953	18	785	160	2536	952	18	784	150
900	7.8	4999	627	9	507	111	3369	622	9	507	106
1500	7.5	4996	628	21	493	91	4001	624	21	492	88

leading to an increase of the reactive probability with respect to QCT. This may be explained as due to the relatively high value of the ZPE in HO_2. In fact, during the collisional process, the vibrational energy of the HO_2 is partially transferred to translation of the system and therefore many of the nonreactive HO_2 molecules will be left behind with a vibrational energy below its starting ZPE value.

The ro-vibrational distributions of the OH and SO products are shown in Fig. 3. The left-hand-side and central panels refer to the results of specific calculations for translational energies of $E_{tr} = 0.2$ and $E_{tr} = 10.0$ kcal mol^{-1}. In turn, the right-hand-side panels show the results obtained for the thermalized calculations at $T = 300$ K. Note that the bottom plots refer to rotational distributions, whereas the upper ones are for the vibrational populations. The notable feature from this figure is, perhaps, the fact that a high rotational energy content is deposited in the newly formed SO. This has been rationalized from a detailed study of the atomic rearrangements along reactive trajectories. To produce OH and SO, we first observe that the sulfur atom attacks the terminal oxygen atom in HO_2. Once the sulfur atoms gets attached to the oxygen one, they start to describe a rotation-like motion around the axis defined by the OH bond. Such a process corresponds to falling into the minimum of the energy path illustrated in Fig. 1. As the SO bond gets shorter and the two oxygen atoms get separated, the sulfur atom maintains this revolving motion with the SO pair separating away with a relatively high content of rotational excitation. Meanwhile, the OH bond remains almost as a spectator, keeping its ro-vibrational distribution as originally was in HO_2. Similar results have been observed for the reaction O + HO_2 when O_2 is formed [22] with a high rotational temperature.

For the thermalized calculations at $T = 1500$ K, part of the vibrational energy is initially deposited into the OH vibrational mode, with this bond showing no longer a spectator behavior. As a result, the HS + O_2 channel opens: six trajectories in a total of 4996. Such a process occurs via an isomerization of HOO into H···OO (see Table 5 of [8]) and continues with the capture of the quasi-free hydrogen atom by the sulfur one. As expected from this analysis, the H + S + O_2 products are also obtained under such conditions, with almost three times more occurrences (17 trajectories) than the diatom–diatom process referred to above. Of course, both processes are statistically negligible when compared with formation of OH + SO (493 trajectories).

Figure 4 shows the predicted excitation functions for the specific calculations. Total reactive and OH + SO formation cross sections are displayed. In turn, the

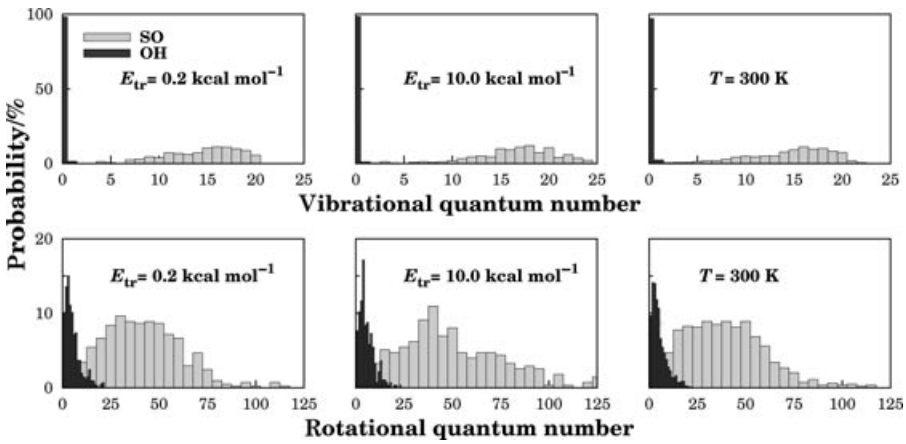

Figure 3 Ro-vibrational distributions of the OH and SO products. Left-hand-side and central panels show quantum number populations for specific calculations at $E_{tr} = 0.2$ and 10 kcal mol^{-1}, respectively. Panels on the right-hand side stand for thermalized calculations at $T = 300$ K.

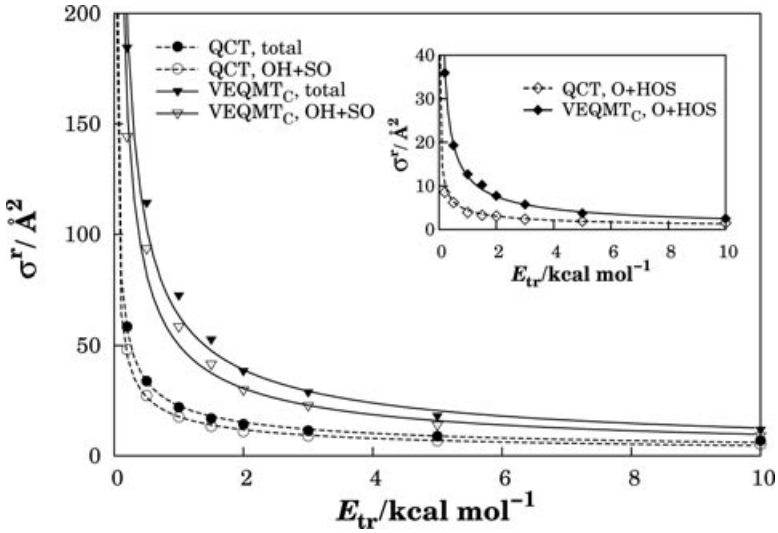

Figure 4 Reactive QCT and VEQMT$_C$ cross sections (total and OH + SO formation) for the title reaction. Also shown in the insert is the cross section for HOS + O formation.

insert shows the corresponding reactive cross section for H + SO_2 formation. As already noted in previous paragraphs, the QCT results are smaller than the VEQMT$_C$ ones, as the latter lead to a higher reactivity. According to the above results and the shape of the potential energy surface (a representative view is the minimum energy paths shown in Figs. 1 and 2), the title reaction is largely controlled by long-range interactions, mainly associated with the permanent electric quadrupole of sulfur and the multipoles of HO_2. Thus, the total reactive cross section and corresponding results for specific channel may be approximated by means of the capture cross section [23]

$$\sigma(E_{\rm tr}) = n\pi(n-2)^{(2-n)/n}\left(\frac{C_n}{2E_{\rm tr}}\right)^{2/n} \qquad (7)$$

where C_n and n are coefficients to be fitted. The calculated values are shown in Fig. 4, with the lines indicating the best fits obtained using Eq. (7). For QCT, $n = 3.432$ and $C_n = 6.083$, while $n = 2.805$ and $C_n = 20.977$ for the VEQMT$_C$ results. Note that the dominant long-range energies arise from the permanent electric quadrupole moment of the S atom and the electric permanent dipole and quadrupole moments of HO_2. Thus, one would formally expect a $V \sim R^{-n}$ dependence. However, owing to dispersion (from two- and three-body terms) as well as other attractive forces of short-range type, such a dependence turns out to be somewhat stronger as indicated above.

By substituting Eq. (7) in Eq. (2) and performing the integration, one gets the following analytical expression for the specific rate constant as a function of temperature:

$$k(T) = 2n\pi g_e(T)(n-2)^{\frac{2-n}{n}}\left(\frac{2}{\pi\mu}\right)^{\frac{1}{2}}\left(\frac{C_n}{2}\right)^{\frac{2}{n}} \times \Gamma\left(\frac{2n-2}{n}\right)(k_B T)^{(n-4)/2n} \qquad (8)$$

where $\Gamma(\ldots)$ is the gamma function. Since OH + SO have already been identified to be the main products, only the rate constants accounting for its formation will be presented. In fact, other products have rate constants a few orders of magnitude smaller ($k^{\rm others} \ll k^{\rm OH+SO}$), with the total rate coefficient differing therefore very little from the one for OH + SO formation. Figure 5 shows the specific QCT and VEQMT$_C$ rate constants calculated in the present work. As expected from the corresponding cross sections in Fig. 4, the VEQMT$_C$ curves lie above the QCT ones. The interval defined by the former curves is light shadowed, with the expected value of $k(T)$ resulting from them being expected to lie somewhere between the upper and lower limits so defined. The dark-shadowed region identifies the corresponding results for the thermalized calculations, according to Eq. (6) and Table II. Open circles and dots denote the actually calculated values, whereas the solid line stands for the QCT results as fitted to the Arrhenius-type form $k(T) = AT^n \exp(-mT)$, and the dashed line to the corresponding fit for the VEQMT$_C$ results. Note that the temperature dependence is similar for both calculations. However, the thermalized rate constants are in average five times larger than the specific ones, with the discrepancy becoming more

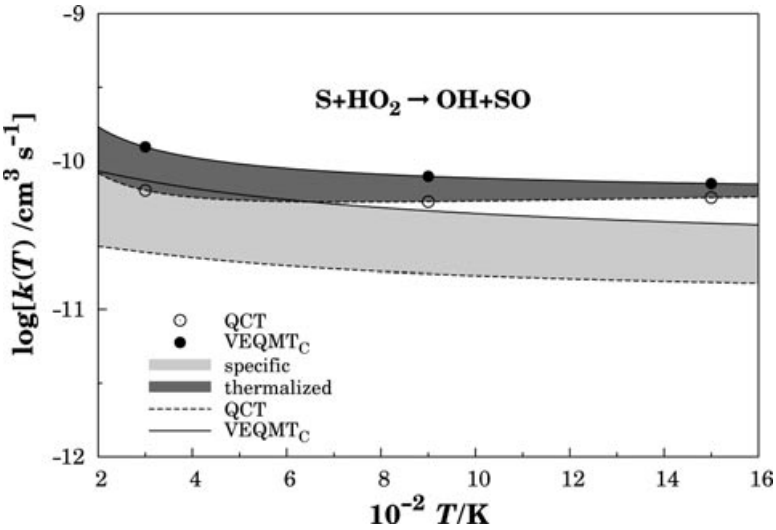

Figure 5 Rate constants for the S + HO_2 → OH + SO reaction. The light-shaded region corresponds to specific ro-vibrational states of the reactants, whereas the dark-shaded area represents the thermalized results. The dashed lines refer to the pure QCT results, whereas the solid ones refer to the $VEQMT_C$ ones. For the thermalized results, the lines indicate Arrhenius-like functions fitted to rate coefficients obtained by QCT and $VEQMT_C$, whose actually calculated values are indicated by open circles and solid dots, respectively.

significant as the temperature rises. As noted above, this is due to the inclusion of vibrational excitation on the thermalized reactants, thus leading to an increase in the reactivity. Because the rotational and vibrational energy of the reactants is properly sampled according to the temperature in the thermalized calculations, our recommended values lie inside the darker region.

Finally, we note that the rate constant obtained in this work for the reaction S + HO_2 → OH + O_2 is $k(T) = 9.4 \times 10^{-11}$ cm^3 s^{-1} at $T = 300$ K, a value quite similar to the one reported [22] for the reaction O + HO_2 → OH + SO, namely $k(T) = (7 - 8) \times 10^{-11}$ cm^3 s^{-1} at the same temperature. More specifically, our recommended value expressed in the Arrhenius form lies between $k(T) = 41.47T^{0.336}\, e^{(245.2/T)} \times 10^{-13}$ cm^3 s^{-1} and $k(T) = 1045.85T^{-0.069}\, e^{(172.1/T)} \times 10^{-13}$ cm^3 s^{-1}, with T in kelvin. The above agreement should not be surprising as O + HO_2 and S + HO_2 have similar bonding characteristics, with a minimum energy path controlled by long-range forces. Indeed, both reaction rate coefficients show a similar dependence on the temperature.

CONCLUSIONS

The S + HO_2 reaction has been studied using two variants of the QCT method. To the best of our knowledge, this is the first study of the dynamics and kinetics of such a reaction. The process has been shown to be dominated by long-range forces, thus manifesting a capture-type behavior. OH + SO has been predicted to be the most formed products channel, although SO_2 and HOS were also formed but with significantly smaller occurrences. Formation of HSO has not been observed. When ZPE leakage is accounted for by the $VEQMT_C$ method, reactivity is favored leading to reactive rate constants larger than in the pure QCT calculations. Calculations using both reactants prepared in specific ro-vibrational states and thermalized ones have been carried out, with larger values of the rate constant predicted for the latter. This is attributed to the fact that vibrationally excited reactants are allowed to occur when preparing the reactants initial states. In both calculations, the formed SO is predicted to be vibrationally hot, similarly to what has been observed [22] for the reaction O + HO_2 → OH + O_2. The calculated rate coefficient is predicted to assume a nearly constant value of $k(T) = 9.4 \times 10^{-11}$ cm^3 s^{-1} for temperatures in the range of $T = 200$–1600 K.

M. Y. B. thanks the Centro de Estudios Ambientales de Cienfuegos, Cuba, for leave of absence during his PhD studies.

BIBLIOGRAPHY

1. Wayne, R. P. Chemistry of Atmospheres, Oxford University Press; New York, 2002.

2. Yamamura, I.; Kawaguchi, K.; Ridgway, S. T. Astrophys J 2000, 528, L33.
3. Alzueta, M. U.; Bilbao, R.; Glarborg, P. Combust Flame 2001, 127, 2234.
4. Ballester, M. Y.; Varandas, A. J. C. Chem Phys Lett 2007, 433, 279.
5. Ballester, M. Y.; Caridade, P. J. S. B.; Varandas, A. J. C. Chem Phys Lett 2007, 439, 301.
6. Varandas, A. J. C. Adv Chem Phys 1988, 74, 255.
7. Varandas, A. J. C. In Conical Intersections: Electronic Structure, Spectroscopy and Dynamics, Advanced Series in Physical Chemistry; World Scientific Publishing: Singapore, 2004; Chap. 5, p. 91.
8. Ballester, M. Y.; Varandas, A. J. C. Phys Chem Chem Phys 2005, 7, 2305.
9. Heinemann, C.; Koch, W.; Lindner, G. G.; Reinen, D. Phys Rev A 1995, 52, 1024.
10. Hase, W. L.; Duchovic, R. J.; Hu, X.; Komornicki, A.; Lim, K. F.; Lu, D.; Peslherbe, G. H.; Swamy, K. N.; Linde, S. R. V.; Varandas, A. J. C.; Wang, H.; Wolf, R. J. QCPE Bull 1996, 16, 43.
11. Varandas, A. J. C.; Brandão, J.; Pastrana, M. R. J Chem Phys 1992, 96, 5137.
12. Truhlar, D. G. J Chem Phys 1972, 56, 3189.
13. Muckerman, J. T.; Newton, M. D. J Chem Phys 1972, 56, 3191.
14. NIST Chemistry WebBook 69, http://webbook.nist.gov/chemistry, 2003.
15. Varandas, A. J. C. Int Rev Phys Chem 2000, 19, 199.
16. Varandas, A. J. C.; Zhang, L. Chem Phys Lett 2001, 340, 62.
17. Varandas, A. J. C. J Chem Phys 1993, 99, 1076.
18. Varandas, A. J. C. Chem Phys Lett 1994, 225, 18.
19. Zhang, D. H.; Zhang, J. Z. H. J Chem Phys 1994, 101, 3671.
20. Varandas, A. J. C.; Pais, A. A. C. C.; Marques, J. M. C.; Wang, W. Chem Phys Lett 1996, 249, 264.
21. Martínez-Núñez, E.; Varandas, A. J. C. J Phys Chem A 2001, 105, 5923.
22. Silveira, D. M.; Caridade, P. J. S. B.; Varandas, A. J. C. J Phys Chem A 2004, 108, 8721.
23. Varandas, A. J. C. In Conferencias Plenarias de la XXIII Reunión Bienal de Química; Feliciano, A. S.; Grande, M.; Casado, J. (Eds.); Universidad de Salamanca: Salamanca, Spain, 1991; p. 321.